METALS AND MATERIALS International, Vol. 11, No. 1 (2005), pp. 53~57

Deformation Behavior of Zr-Based Bulk Metallic Glass in an Undercooled Liquid State under Compressive Loading

Kwang Seok Lee and Young Won Chang*

Center for Advanced Aerospace Materials (CAAM), Pohang University of Science and Technology, Hyoja-dong, Nam-gu, Pohang, Gyeongbuk 790-784, Korea

High temperature deformation behavior of a $Zr_{41.2}Ti_{13.8}Cu_{12.5}Ni_{10}Be_{22.5}$ bulk amorphous alloy has been studied in a temperature range between 355 and 460 °C under compressive loading after rapid heating. A transition of flow behavior, viz. from a Newtonian to a non-Newtonian flow, has been reported by many researchers as the temperature is decreased at a given strain rate. In the present study, two different theoretical relations based on a viscous flow model and a transition state theory have been applied to analyze the transition behavior of deformation in terms of viscosity and flow stress. An experimental deformation map was then constructed to specify the boundaries between Newtonian and non-Newtonian flow, based on the relationship between the flow stress and strain rate in an undercooled liquid state. It has further been confirmed that the stress overshoot phenomena can be observed mostly in a non-Newtonian flow regime appearing in an intermediate temperature and strain rate region in this deformation map.

Keywords: bulk metallic glass, deformation behavior, flow stress, Newtonian viscous flow

1. INTRODUCTION

Transition metal based multi-component alloy systems have been found to vitrify in various bulk forms since they were first reported in 1990 [1-4]. The "bulk" metallic glasses are very important for both scientific studies and industrial applications. It is therefore critical to develop more glass forming alloy systems with slow cooling rates. Recently developed metallic glasses, for an example, have critical cooling rates less than 10^2 K/s, several orders of magnitude slower than that required for most metallic alloys reported to date [2,3,5]. The bulk metallic glass can then be fabricated by processes such as a simple copper mold casting or die-casting under a controlled atmosphere. Utilizing this unique viscous property, bulk metallic glasses can be stamped [6], extruded [7], nano-indented [8], or electrochemically shaped [9] under proper forming conditions. It is, however, necessary to establish the optimum forming conditions while maintaining the characteristic properties of amorphous materials in order to reduce the cost of mass production processes.

Distinct improvements have been made in recently developed bulk metallic glasses with respect to their mechanical properties as well as thermal stability [1]. With regard to mechanical properties, most metallic glasses exhibit respectable strength and ductility under compressive or bend loading as a result of multiple shear band formation or homogeneous viscous flow. The Zr-Ti-based "Vitreloy" series has been reported to have high strength alloy at room temperature [2] with viscous flow characteristics in an undercooled liquid state [10]. These alloys can be used as structural as well as functional materials in amorphous single phase or nano-crystalline embedded multiphase especially due to their high degree of resistance to crystallization.

The deformation mode of bulk metallic glasses generally depends upon temperature and strain rate. At room temperature, most bulk metallic glasses show brittle fracture characteristics caused by unstable flow in the form of shear localization [11]. In contrast, homogeneous flow without brittle fracture can be observed in an undercooled liquid state with severe plastic deformation under proper strain rates. Results have been reported to explain this transition from a Newtonian to a non-Newtonian flow in a homogeneous flow region through investigation of the flow stress variation as a function of temperature and strain rate. The free volume model is widely used to explain the softening mechanism for an inhomogeneous flow and deformation-induced structural disordering [12]. Newtonian viscosity is often described by the well-known Vogel-Fulcher-Tammann (VFT) equation to cover a broad temperature range of melt and undercooled liquid [13] or the Cohen-Grest (CG) model [14]. A transition state theory is also applicable for the Norton plot including non-Newtonian flows [15,16]. Recently, a self-consistent dynamic free vol-

*Corresponding author: ywchang@postech.ac.kr

ume (SCDFV) model has been proposed to establish a shear-rate dependent constitutive law applicable in both the Newtonian and non-Newtonian flow regimes [17].

In the present work, the effect of temperature and strain rate on the deformation behavior of $Zr_{41.2}Ti_{13.8}Cu_{12.5}Ni_{10}Be_{22.5}$ (Vitreloy 1) bulk metallic glass has been investigated by conducting a series of compression tests within an undercooled liquid region. The viscosity model for uniaxial deformation and the transition state theory were found to fit the steady-state flow stress reasonably well. From these fitting curves obtained by the viscosity and transition state equations, a deformation map was constructed in terms of processing temperature and strain rate, including the boundaries between Newtonian and non-Newtonian flow.

2. EXPERIMENTAL PROCEDURE

Plate-type bulk amorphous ingots of $Zr_{41.2}Ti_{13.8}Cu_{12.5}Ni_{10}Be_{22.5}$ (at.%), originally developed by the W. L. Johnson group at CALTECH [2], were obtained from Liquidmetal Technologies, Co. with dimensions of 80 mm×100 mm×3 mm. The formation of a single amorphous phase was confirmed through a typical amorphous X-ray diffraction pattern as well as a high-resolution electron microscopy (HREM). There was no sign of sharp Bragg peaks. Rectangular shaped samples with a cross-section of 3×3 mm^2 and a height of 6 mm were obtained by electrical discharge machining and then carefully polished. A series of compression tests was then conducted using a computer controlled electro-mechanical testing machine (INSTRON 1361) equipped with a high temperature halogen furnace capable of rapid heating. The load vs. time data were monitored and stored through a digital voltmeter (IOTECH DAQBOOK) to generate the true stress-strain curves. These compression tests were performed within a temperature range of 355 to 460 °C under initial strain rates ($\dot{\varepsilon}$) ranging from 3×10^{-5}/s to 1×10^{0}/s after holding for 3 min at a given test temperature. To determine the exact test temperature and pre-annealing time, continuous heating and isothermal annealing were then performed in a differential scanning calorimetry (DSC). Continuous heating was carried out with a heating rate of 20 °C/min in an argon atmosphere. The glass transition temperature (T_g) and the onset temperature for crystallization (T_x) were thereby determined to be 355 and 456 °C, respectively. Fig. 1(a) shows the isothermal annealing curves obtained by DSC at various temperatures in an undercooled liquid state, revealing two different types of isothermal crystallization curves. Two distinct exothermic peaks are observed at higher holding temperatures above 420 °C, while a single exothermic peak is seen below 410 °C after some incubation time. The experimental time-temperature-transformation (TTT) diagrams are plotted in Fig. 1(b) for the two different crystallization steps in an undercooled liquid state.

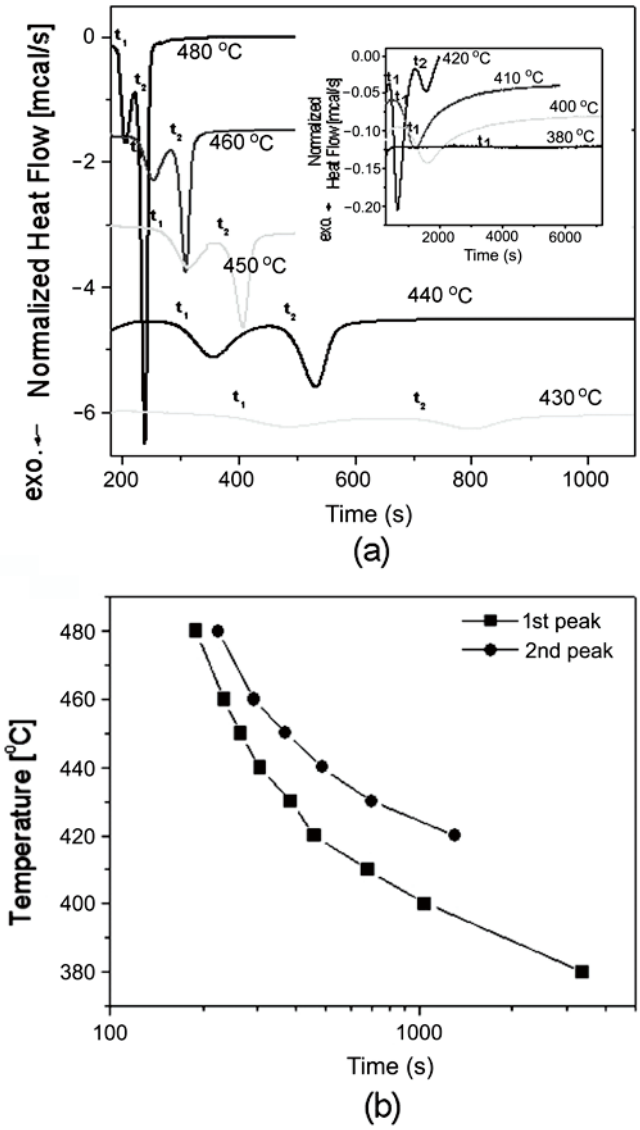

Fig. 1. (a) Isothermal DSC curves at various annealing temperatures and (b) Experimental TTT diagrams for the first and second crystallization peaks of $Zr_{41.2}Ti_{13.8}Cu_{12.5}Ni_{10}Be_{22.5}$ bulk amorphous alloy.

3. RESULTS AND DISCUSSION

3.1. Compressive deformation behavior

The true compressive stress-strain curves obtained under various strain rates at 370 and 400 °C for this bulk amorphous alloy are shown in Fig. 2. The curves are shifted slightly along the strain axis by the true strain values ranging from 0 to 0.03 for an easier comparison. The transition behavior in deformation from a shear failure to a homogeneous flow can be observed at these temperatures. A linear viscoelastic flow without a stress overshoot is exhibited for the case of $\dot{\varepsilon}=3\times10^{-5}$/s at 370 °C in Fig. 2(a). It is, however, clear from the figure that the increase in strain rate leads the transition in deformation mode into a nonlinear viscoelastic

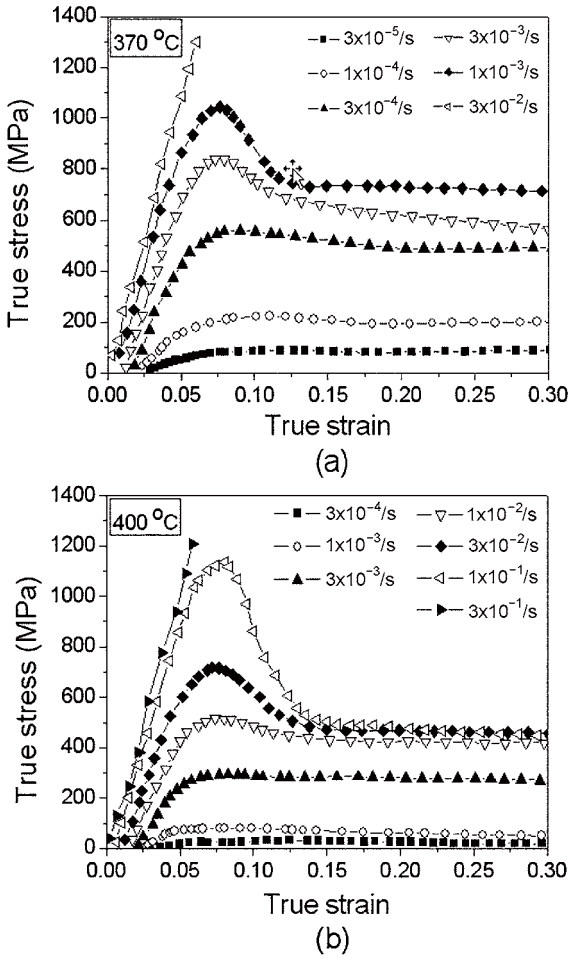

Fig. 2. Uniaxial true stress-strain curves obtained with various strain rates at temperatures of (a) 370 °C and (b) 400 °C.

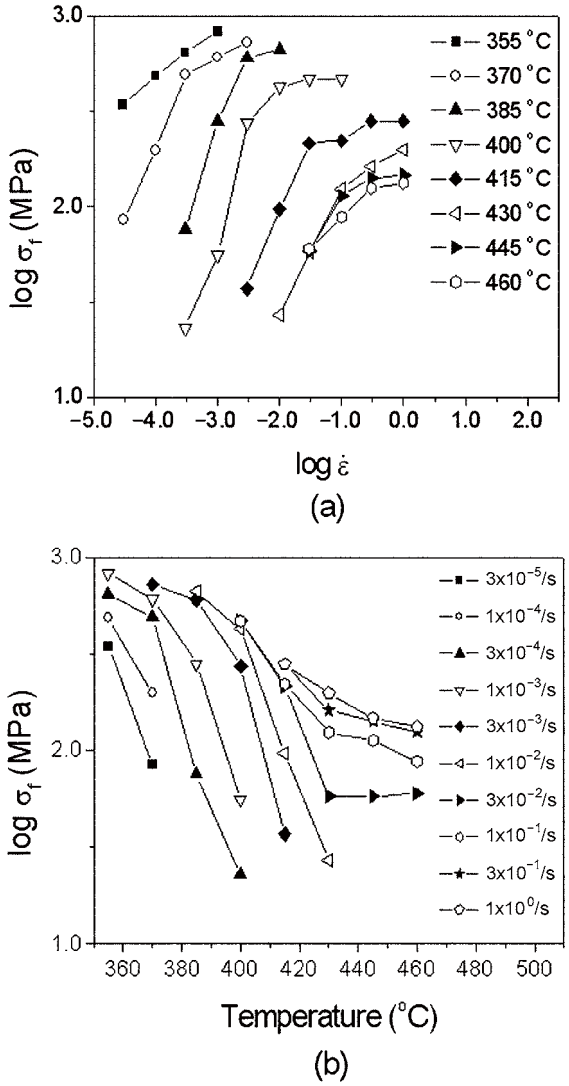

Fig. 3. The variations of steady-state flow stresses (σ_f): (a) at various test temperatures as a function of initial strain rate and (b) at various initial strain rates as a function of test temperature.

flow with an increasing amount of stress overshoot up to the rate of $\dot{\varepsilon}=3\times10^{-3}$/s. Brittle fracturing caused by localized shear failure occurred without any plastic flow at the faster strain rate of $\dot{\varepsilon}=1\times10^{-2}$/s. The alloy also shows a Newtonian viscous flow with extremely low flow stress, less than 80 MPa, at sufficiently low strain rates below 1×10^{-3}/s at 400 °C, as can be seen in Fig. 2(b). At 400 °C, the critical initial strain rates for non-linear viscoelastic flow and brittle fracture are found to increase compared with those at 370 °C. Meanwhile, a brittle fracture mode could not be observed at the strain rate range from 3×10^{-3}/s to 1×10^{0}/s at higher temperatures above 415 °C.

From the above observations, three different types of true stress-strain curves can be identified under compressive loading within the undercooled liquid region depending on the strain rates and test temperatures. The first mode shows a large viscous flow without stress overshoot, implying a Newtonian viscous flow typically observed at lower strain rates and higher temperatures. Mode II, a steady-state flow after stress overshoot, was observed at intermediate temperatures and the medium strain rate region, while mode III was characterized by brittle fracture caused by shear localization at lower temperatures and in the faster strain rate region.

The steady-state flow stresses (σ_f) are plotted as a function of strain rate for various test temperatures in Fig. 3(a). At 355 °C, close to the glass transition temperature, the relationship between log σ_f and loge shows monotonously increasing single-step linearity. The steady-state flow stresses at the temperatures above 370 °C are observed to increase linearly with a relatively steeper slope at lower strain rates, implying higher strain rate sensitivity values compared to that of the higher strain rate region. It is, however, also noted that the rate of increase in steady-state flow stress decreases as the strain rate increases further to the final fracture due to shear failure. Therefore, the double log plots of σ_f vs. $\dot{\varepsilon}$ exhibit a bend-over with two distinctly different flow modes. The variation of σ_f is

also plotted in Fig. 3(b) with respect to the test temperatures at the various initial strain rates. At the intermediate temperature range in an undercooled liquid state, σ_f is seen to decrease drastically with temperature increase for a given initial strain rate. The rate of decrease of σ_f is found to lessen significantly at higher temperatures above 430 °C.

3.2. Transition of deformation mode

As manifested by the compressive stress-strain curves, the deformation behavior of metallic glasses can be described in two different regions depending on the processing conditions such as strain rate and temperature. A homogeneous flow, where each unit volume of a specimen contributes to the strain, is observed to occur at sufficiently low stresses levels, while an inhomogeneous flow, leading to brittle fracture without appreciable plastic flow, is seen to occur at higher stresses and lower temperatures. This inhomogeneous flow appears relatively insensitive to the test temperature and strain rate. The steady-state flow stresses obtained at 370 and 430 °C are plotted in terms of the applied strain rate in Fig. 4 and analyzed based on the homogeneous flow model including Newtonian viscous and non-Newtonian flows. The strain rate sensitivity parameter, m (=$\Delta \log \sigma_f / \Delta \log \dot{\varepsilon}$), appears nearly equal to 1.0 in the low stress and low strain rate regime. The value of m is observed to decrease significantly to 0.2 or lower in the high stress and high strain rate regime. The transition of m value observed in this study is in good agreement with that previously reported for another Zr-based metallic glass system by A. Reger-Leonhard *et al*. [18].

According to the transition state theory of flow stress, originally suggested by F. Spaepen [19], the steady-state flow stress is described by Eq. 1

$$\dot{\varepsilon} = \dot{\varepsilon}_0 \sinh \frac{\sigma_f \gamma_0 \Omega_f}{M k_b T} \tag{1}$$

with $\dot{\varepsilon}_0$ denotes the reference strain rates, γ_0 the local strain, Ω_f the shear site of volume, and $M=\sqrt{3}$ for uniaxial deformation. The solids lines in Fig. 4 represent the results predicted by Eq. 1 with the two fitting parameters of $\gamma_0\Omega_f$ and $\dot{\varepsilon}_0$, suggesting that this transition state theory is applicable only in the high strain rate and high stress regime. It is, therefore, thought here that the deformation behavior in the high stress-high strain rate regime might be described by the transition state theory appropriate for a non-Newtonian flow.

A significant deviation from the data can be seen in the low strain rate and low stress regime, suggesting a different deformation mode in this regime. For an ideal Newtonian viscous flow, the shear stress is proportional to the velocity gradient with a proportionality constant η, usually defined as the viscosity, to provide the relation between σ_f and $\dot{\varepsilon}$ under a uniaxial deformation condition,

$$\sigma_f = 3\eta\dot{\varepsilon} \tag{2}$$

The dotted lines in Fig. 4 represent the predicted flow obtained by Eq. 2. In this low stress and low strain rate regime, Newtonian viscous flow appears to be dominant with the value of viscosity remaining as the nearly constant value of a steady-state Newtonian viscosity, η_N.

The log σ_f vs. log $\dot{\varepsilon}$ data obtained at various test temperatures are plotted together with the predicted curves obtained using Eqs. 1 and 2 in Fig. 5, exhibiting fairly good agreement over a wide range of test temperatures. Based on the above classification of deformation mode of metallic glasses, an empirical deformation map can be constructed separating the homogeneous viscous flow region from the inhomogeneous flow region in terms of strain rate and processing temperature [19]. There have only been, however, limited reports to date on the deformation map for metallic glasses due to ambiguity regarding the method of determining the division between Newtonian viscous and non-Newtonian flows in a homogeneous flow regime. In the present study, three distinctly different deformation modes were identified as described previously depending on the strain rate and test temperature.

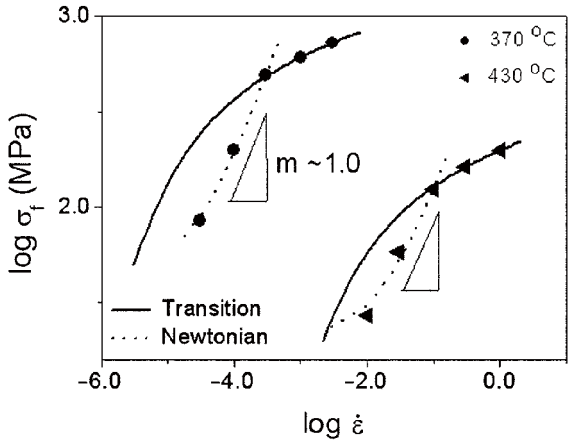

Fig. 4. Steady-state flow stress (σ_f) and strain rate relationship at 370 and 430 °C.

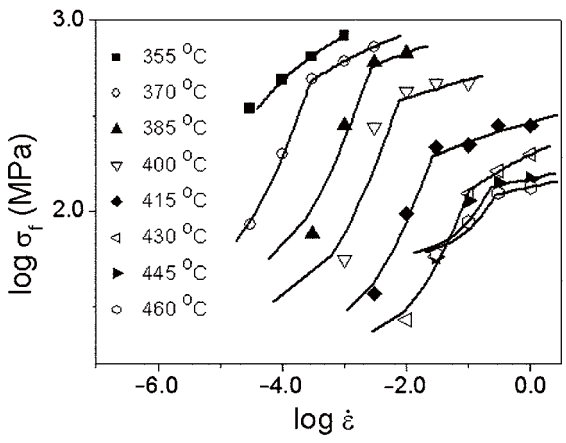

Fig. 5. Steady-state flow stress vs. strain rate relations at various temperatures.

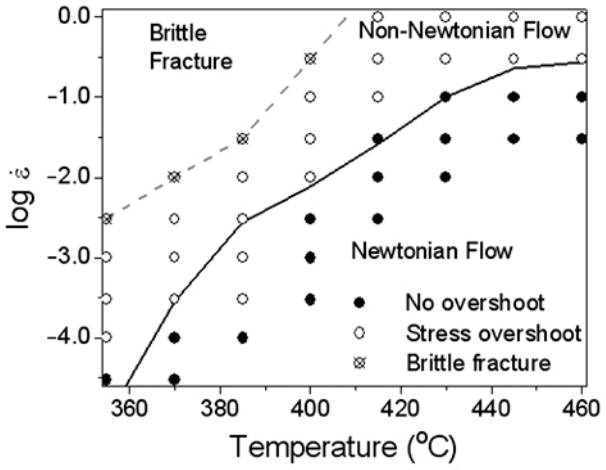

Fig. 6. An empirical deformation map constructed from the compression test results.

It is thus possible to construct the empirical deformation maps given in Fig. 6, exhibiting the characteristic processing conditions for each deformation mode. The solid line in the figure represents the boundary between a Newtonian and a non-Newtonian viscous flow, determined as the intersection points of the two predicted curves given in Fig. 5. These points can in fact be interpreted as the critical strain rates for a Newtonian flow at a given temperature. The dotted line in the figure denotes the experimental boundary between a non-Newtonian homogeneous flow and an inhomogeneous flow leading to shear failure. The solid, open, and open-crossed circles in Fig. 6 represent a linear viscoelastic flow without stress overshoot, a non-linear viscoelastic flow with stress overshoot, and a brittle fracture without plastic flow, respectively. The regions of Newtonian flow, non-Newtonian flow, and brittle fracture seem to correspond well with those of linear viscoelastic flow, non-linear viscoelastic flow, and shear failure, respectively, except for some data at 385 °C. The stress overshoot phenomena observed in the homogeneous flow regime can thus be regarded as a criterion for a non-Newtonian flow.

4. SUMMARY

A series of compression tests has been conducted for a bulk amorphous $Zr_{41.2}Ti_{13.8}Cu_{12.5}Ni_{10}Be_{22.5}$ alloy in an undercooled liquid state. The results obtained are summarized as follows:

(1) Three distinctly different types of stress-strain curves are observed depending on the strain rate and test temperature. A viscous flow without stress overshoot was observed at high temperature and low strain rate region, while a non-linear viscoelastic flow with stress overshoot was observed at intermediate temperature and intermediate strain rate region. The third type, viz. brittle fracture without plastic flow, was observed at low temperature and high strain rate region.

(2) The homogeneous flow regime in an undercooled liquid state was found to separate into two different regions except at 355 °C, viz. a Newtonian viscous flow region with a strain rate sensitivity parameter close to 1.0 in a low stress and low strain rate region and a non-Newtonian flow with drastically reduced strain rate sensitivity values in a high stress and high strain rate region.

(3) The homogeneous flow could be described by combining the transition state theory and a Newtonian viscosity model for uniaxial deformation. As a result, an empirical deformation map could be constructed providing the boundaries between the different deformation modes depending on the processing conditions.

ACKNOWLEDGMENT

The 2003 National Research Laboratory (NRL) Program of the Korea Ministry of Science and Technology supported this work and the authors are grateful for that.

REFERENCES

1. A. Inoue and A. Takeuchi, *Mater. Sci. Eng. A* **375-377**, 16 (2004).
2. A. Peker and W. L. Johnson, *Appl. Phys. Lett.* **63**, 2342 (1993).
3. D. S. Sung, O. J. Kwon, E. Fleury, K. B. Kim, J. C. Lee, D. H. Kim, and Y. C. Kim, *Met. Mater. -Int.* **10**, 575 (2004).
4. W. B. Kim, B. J. Ye, and S. Yi, *Met. And Mater Int.* **10**, 1 (2004).
5. N. Nishiyama and A. Inoue, *Appl. Phys. Lett.* **80**, 568 (2002).
6. K. S. Lee, W. Bang, T. K. Ha, S. Ahn, and Y. W. Chang, *J. Metastable Nanocryst. Mater.* **15-16**, 155 (2003).
7. Y. Kawamura, T. Shibata, A. Inoue, and T. Masumoto, *Acta mater.* **46**, 253 (1998).
8. Y. Saotome, T. Hatori, T. Zhang, and A. Inoue, *Mater. Sci. Eng. A* **304-306**, 716 (2001).
9. A. R. Yabari, M. F. de Oliveira, C. S. Kiminami, A. Inoue, and W. J. Botta F., *Mater. Sci. Eng. A* (in press).
10. K. S. Lee, T. K. Ha, S. Ahn, and Y. W. Chang, *J. Non-cryst. Sol.* **317**, 193 (2003).
11. M. D. Demetriou and W. L. Johnson, *Acta mater.* **52**, 3403 (2004).
12. P. de Hey, J. Sietsma, and A. van den Beukel, *Acta mater.* **46**, 5873 (1998).
13. M. Cohen and D. Turnbull, *J. Chem. Phys.* **31**, 1164 (1959).
14. M. Cohen and G. Grest. *J. Non-cryst. Solids* **61**, 749 (2003).
15. A. I. Taub, *Acta metall.* **28**, 633 (1980).
16. A. I. Taub and F. E. Luborsky, *Acta metall.* **29**, 1939 (1981).
17. W. L. Johnson, J. Lu, and M. D. Demetriou, *Intermetallics* **10**, 1039 (2002).
18. A. Reger-Leonhard, M. Heilmaier, and J. Eckert, *Scripta mater.* **43**, 459 (2000).
19. F. Spaepen, *Acta metall.* **25**, 407 (1977).